STATUS OF THE MINOS EXPERIMENT

R. BERNSTEIN for the MINOS Collaboration
FermiLab
Batavia, IL 60510 USA
E-mail: rhbob@fnal.gov

ABSTRACT

We discuss the status of the MINOS experiment. The plans for different beams, the likely reach, and the expected schedule are given.

1. Introduction and Physics Goals

MINOS is a long-baseline neutrino oscillation experiment using the Fermilab Main Injector. It will send a beam of neutrinos of energies from 1–20 GeV to the Soudan Underground Laboratory 732 km away in Tower, Minnesota. The experiment will use two detectors, one located on the FNAL site and a second at the Soudan Lab in order to measure the intial flux and compare to the composition at the far detector. The initial beam is almost pure ν_μ and the primary goal of MINOS is to search for $\nu\mu \to \nu_\tau$ oscillations in the region of parameter space indicated by the Atmospheric Neutrino Deficit.[1)]

The experiment will use one of three beams which differ in the arrangement of the focusing horns. They are designed to produce neutrino interactions at Soudan roughly in the 2–5 (PH2l),5–7 (PH2m), and 10–15 GeV (PH2) ranges. The experiment can then be exposed to different energies depending upon our accumulating knowledge of Δm^2.

Table 1 gives a quantitative summary of the physics goals.

Measurement	Sensitivity (90% CL)
$\nu_\mu \to \nu_\tau$ limit, high Δm^2	$\sin^2(2\theta) > 1.9 \times 10^{-2}$ (NC/CC test)
$\nu_\mu \to \nu_\tau$ limit, $\sin^2(2\theta) = 1$, high energy beam	$\Delta m^2 > 2 \times 10^{-3}$ eV^2 (NC/CC test)
$\nu_\mu \to \nu_\tau$ limit, $\sin^2(2\theta) = 1$, low energy beam	$\Delta m^2 > 6 \times 10^{-4}$ eV^2 (ν_μ disappearance)
$\nu_\mu \to \nu_\tau$ limit, $\sin^2(2\theta) = 1$, τ identification	$\Delta m^2 > 1.7 \times 10^{-3}$ eV^2 (ν_τ CC events)
$\nu_\mu \to \nu_e$ limit, high Δm^2	$\sin^2(2\theta) > 2 \times 10^{-3}$ (ν_e appearance test)
$\nu_\mu \to \nu_e$ limit, $\sin^2(2\theta) = 1$	$\Delta m^2 > 3 \times 10^{-4}$ eV^2 (ν_e appearance test)
Δm^2 measurement precision	1×10^{-3} eV^2 for $\Delta m^2 = 10^{-2}$ eV^2
$\sin^2(2\theta)$ measurement precision	1×10^{-1} for $\Delta m^2 = 10^{-2}$ eV^2
Limit on admixture of $\nu_\mu \to \nu_e$, $\nu_\mu \to \nu_\tau$	$\sin^2(2\theta) < 0.06$ for $\Delta m^2 = 10^{-2}$ eV^2

Table 1: MINOS physics goals. The experiment will achieve these sensitivities in a two year run. If oscillations are not found, the 90% confidence level limits shown will be achieved. If oscillations are observed with $\Delta m^2 = 10^{-2}$ eV^2, the parameters and modes will be determined with the indicated precisions.

If oscillations occur, the experiment must be able to measure the parameters and distinguish between different oscillation modes. This requires good energy resolution for hadrons, muons and electrons, and the ability to distinguish the topologies of ν_μ, ν_e, and ν_τ interactions. These requirements determine the transverse and longitudinal granularities and the magnetic field strength; however, sensitivities depend rather weakly on these parameters. Calibration of the relative energy scales of the near and far detectors is important for the determination of Δm^2. Good hadronic energy resolution is also important for this measurement; good electromagnetic energy resolution is needed for ν_e identification and parameter measurement if $\nu_\mu \to \nu_e$ oscillations occur. The explicit identification of the decays of τ leptons from ν_τ charged current interactions, via statistical analyses, puts stringent demands on several detector parameters: longitudinal and transverse granularities, π^o/electron identification and the tails of the calorimetric energy response. Our design is conservative with regard to Δm^2 sensitivity: we have chosen detector parameters which will retain good event identification and measurement capabilities should it turn out to be advisable, for physics reasons, to run at lower beam energies than the default high-energy wide-band beam. Table 2 summarizes the experimental parameters of the MINOS design.

Parameter	Value
Near detector mass	0.98 (metric) kt total, 0.1 kt fiducial
Far detector mass (2 supermodules)	5.4 (metric) kt total, 3.3 kt fiducial
Steel planes (far detector)	8-m wide, 2.54-cm thick octagons
Magnetic field (far detector)	Toroidal, 1.5 T at 2 m radius
Active detector planes	Extruded polystyrene scintillator strips
Active detector strips	4.1-cm wide, 1-cm thick, ∼8-m long
Near detector distance from decay pipe	290 m
Far detector distance from decay pipe	730 km
Cosmic ray rates	270 Hz in near det., 1 Hz in far det.
Neutrino energy range (3 configurations)	1 to 25 GeV
Detector energy scale calibration	5% absolute, 2% near-far
Detector EM energy resolution	$23\%/\sqrt{E}$ (<5% constant term)
Detector hadron energy resolution	$60\%/\sqrt{E}$ (<7% constant term)
Detector muon energy resolution	<12% (from curvature or range)
NC-CC event separation	Efficiency >90%, correctable to 99.5%
Electron/π separation	Hadron rejection $\sim 10^3$ for ϵ_e ∼20%
Far det. ν event rate (high-energy beam)	3000 ν_μ CC events/kt/yr (no oscillations)
Near det. ν event rate (high-energy beam)	20 events/spill in target region
Near-far relative rate uncertainty	2%

Table 2: MINOS experimental parameters with the highest-energy wide-band beam.

2. Beams

The primary 120 GeV protons will be extracted from the Main Injector using the standard resonant extraction technique over a time period of 1 msec. Next, they will be transported to the downstream target hall and aimed downwards at 3.3° so as to point at the MINOS far detector on the lowest level of the Soudan mine. By 2002 the Main Injector is expected to deliver about 4×10^{13} protons per pulse on target.

The target design optimizes neutrino yield but also takes into account the need to have a conservative design that can withstand the proton beam intensities contemplated. The target is a small diameter (matched to the transverse size of the proton beam) segmented graphite or beryllium cylinder about 160 cm long. The gaps between the segments allow most of the produced pions and kaons to leave the target before interacting. A 0° targeting angle will be used for the wide-band beam (WBB) configurations considered here.

The resulting hadron beam is subsequently sign selected and focused by specially designed focusing elements and then transported through an evacuated decay pipe, 1 m in radius and 675 m long, before striking a secondary hadron absorber downstream. Including the 50 m distance between the production target and the decay pipe, the total decay length is 725 m.

Figure 2 displays the calculated performance of this parabolic horn NuMI beam. The upper curve, corresponding to perfect focus and a 675 m long decay pipe, shows the maximum interacting neutrino spectrum theoretically available, given the Main Injector proton intensity and the proposed NuMI target. The lower three curves show the event rate as a function of energy for three different configurations of the beam. About 3000 ν_μ CC events/kt/year are expected in the MINOS far detector for the highest energy configuration.

3. The near detector

The primary function of the near detector is to serve as a reference for the principal MINOS (far) detector in the Soudan mine. Our philosophy is to obtain a direct measurement of the rates and characteristics of the neutrino interactions before the neutrinos have had a chance to oscillate. The measurements can then be compared with the equivalent measurements at the far detector to see if oscillations have occurred. The dependence on Monte Carlo calculations is greatly reduced by comparing far detector data to near detector data instead of making comparisons to Monte Carlo predictions. For such a comparison to be most useful, the beam and detector characteristics at the two locations, as well as the experimental environment, have to be as similar as possible and their differences well understood.

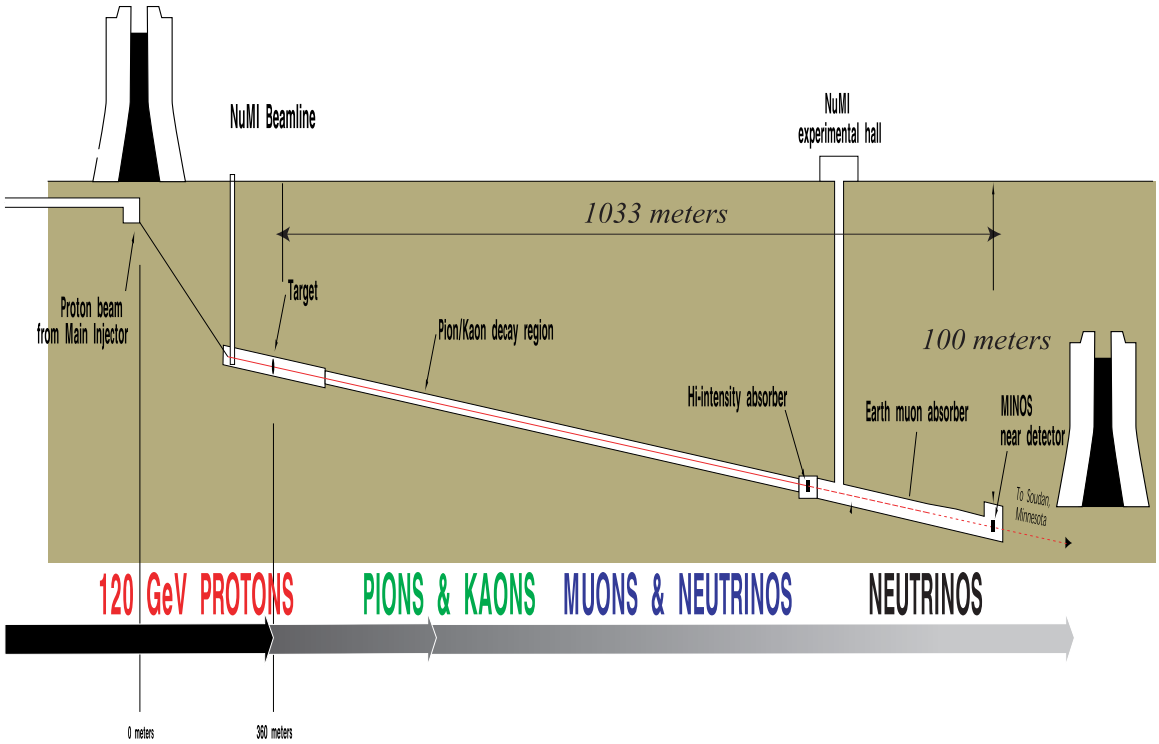

Figure 1: Map of the Fermilab site, showing the NuMI beamline and the approximate locations of the hadron absorber and the MINOS near hall.

There are several differences, however, that cannot be eliminated:

a) The neutrino energy spectrum at the two locations will be somewhat different. This is due to the finite length of the neutrino source. This length is comparable to the distance between a typical π or K decay point and the near detector. The "size" of the beam differs as well — the spectrum is essentially identical everywhere in the far detector but varies in the near location.

b) The neutrino flux is significantly higher at the near detector.

c) The near detector is at a shallower depth than the far detector.

The beam spectra differences are due to π and K decay kinematics (a neutrino emitted at a larger angle has lower energy) and the fact that lower energy neutrinos tend to be produced further upstream (due to shorter parent lifetime). Thus the differences are easily understood. In addition, if we use neutrino events from only the central beam region of the near detector (we plan to use r $<$ 25 cm), the differences are minimized.

Flux differences at the two locations are not a problem if pileup and overlap rates are kept low, as is the case in our experiment.

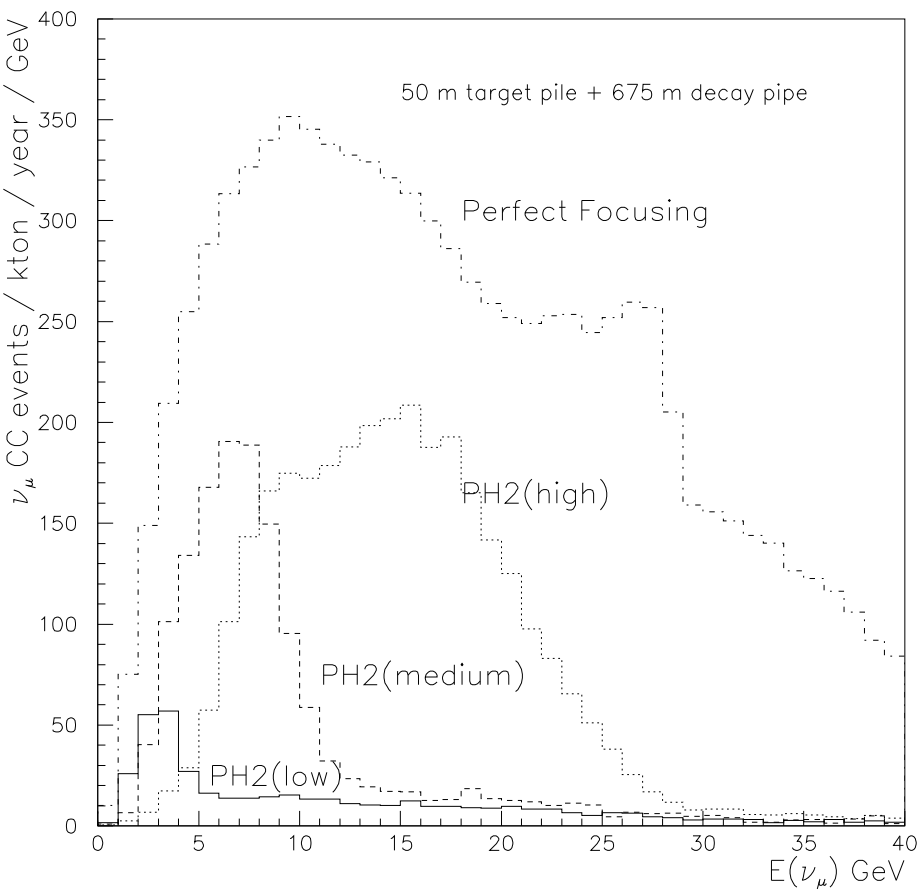

Figure 2: Neutrino interaction energy spectra predicted for different beam focusing conditions. 'Perfect Focusing' assumes all secondary charged particles (with the proper sign) from the target are focused into a pencil beam with no divergence. 'PH2(high),' 'PH2(medium)' and 'PH2(low)' are the high, medium and low energy configurations of the parabolic horn beam.

Finally, the near and far detectors have different cosmic ray rates because of their different depths. Although the ratio of rates is quite large, the absolute rates at both locations are still quite low ($1.8 \times 10^{-3}/\mathrm{m}^2/\mathrm{s}$ at Soudan and $1.6\ /\mathrm{m}^2/\mathrm{s}$ in the near detector cavern). The low beam duty cycle, $<10^{-3}$, reduces the impact of cosmic rays even further and allows a very accurate measurement of the effect of any residual cosmic ray background.

The design of the near detector attempts to emulate that of the far detector in all relevant properties: the nature and thickness of absorber planes, the nature and granularity of the active detector, and the strength of the magnetic field. The basic near-detector shape is an elongated octagon, 3.8 m high and 4.8 m wide, as shown in Figure 3. The coil hole is placed off center horizontally, and the detector itself is positioned so that the central part of the neutrino beam is about 1 m away from the hole. This geometry was chosen to minimize the amount of steel used while still providing a sufficient steel plane area with an adequate magnetic field in the neutrino interaction region.

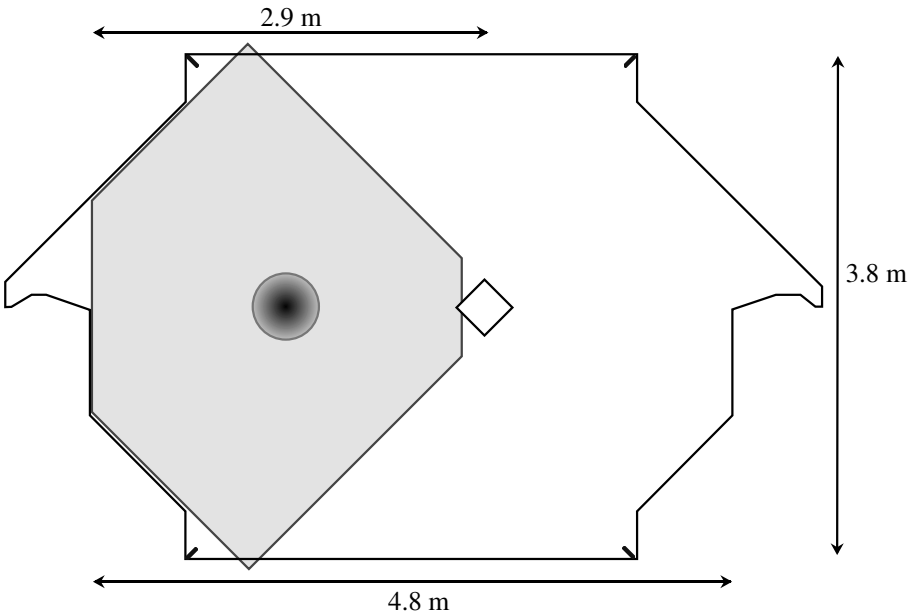

Figure 3: Sketch of a partially instrumented near detector plane in one of the three upstream sections, showing the area instrumented with scintillator strips. The central square represents the magnet coil hole and the circle shows the 25 cm radius central beam region. The shaded area is covered with scintillator strips and the rest of the steel plate is uncovered. Each strip is read out from its outer end only.

In the longitudinal dimension, the detector is composed of four functionally different components. Starting from the upstream end, they are:

a) **Veto** This is the upstream part of the detector whose neutrino interactions are

not used, because of possible end effects and the need to assure that there is no background from neutron interactions. The veto part also assures that the following target region has no anomalous end effects. This part has a thickness of 0.5 m of steel.

b) **Target** Neutrino interactions in this part are used for the near/far comparison. It has a thickness of 1.0 m of steel.

c) **Hadron Shower Detector** This part has to be long enough to contain the full showers of all neutrino interactions occurring in the target part. It has a thickness of 1.5 m of steel.

d) **Muon Spectrometer** This part is used to range out muons and/or measure their momentum by curvature. The length is determined by the momentum accuracy needed to match that of the far detector; 4 m of steel is sufficient for this.

Figure 4 shows the layout of the near detector in the longitudinal direction. The first three parts, although functionally different, are identical in the active detector technology used and their transverse and longitudinal granularities. They are also identical to the far detector in these respects. Because the accuracy of muon measurement by curvature is determined by Coulomb scattering in steel (for sufficiently long traversals, as is the case here), the requirements on the detector elements in the muon spectrometer are less stringent than in the three upstream parts. We therefore use active detectors only on every fourth plane of steel in this part.

As mentioned above, we plan to use only the central part of the neutrino beam ($r < 25$ cm) for the near/far comparison. Because the transverse spread of a hadronic shower is about half a meter at our energies and in our detector, we need to instrument only a part of the area of the upstream sections of the near detector. In order to measure the neutrino spectrum out to about 1 m from the axis, we will instrument an area of 2.8 m by 2.8 m in this region. In addition, every fifth scintillator plane in the first three sections will have a larger instrumented area to indicate the presence of tracks and interactions outside the central beam area.

The instrumentation of the near detector is very similar to that of the far detector; the basic detector elements are 4-cm wide scintillator strips with a wavelength shifting fiber imbedded in them. Because of the higher rates and the smaller number of channels, we will read out each scintillator strip in the three upstream sections separately, without the multiplexing scheme used in the far detector. Most scintillator planes in the upstream part of the detector cover only about one quarter of the steel plane area, as indicated in Figure 3. The length of the strips is variable, corresponding to the shape of the iron, and ranges from 1.5 to 2.7 m in length. In the muon spectrometer part, the full area of the steel planes is covered with scintillator

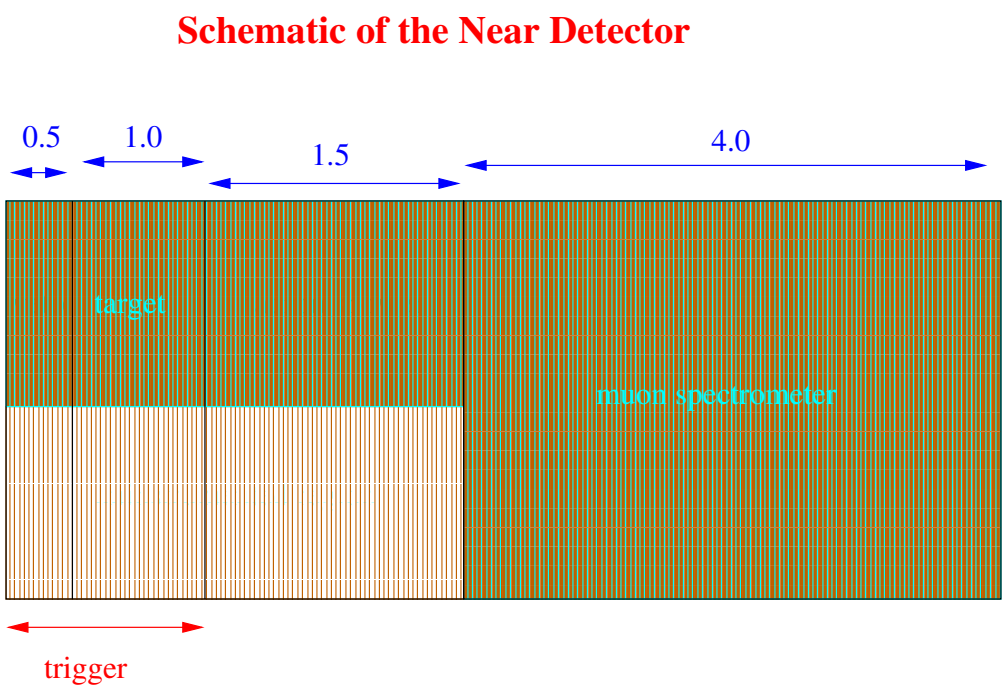

Figure 4: Schematic representation of the four functional parts of the MINOS near detector. The thicknesses shown (in meters) are only for the steel planes, and do not include the space occupied by detector planes. The beam enters from the left and is centered on the shaded region. Shading is used to indicate instrumented regions of the detector.

and 4× multiplexed readout is used. All near detector strips are read out from only one end and the orientation of strips alternates in successive planes.

Although the rates in the near detector are considerably higher than in the far detector, they do not introduce any significant dead time, pileup, or event overlap problems. The singles rate in the detector comes mainly from the neutrino interactions in the detector and from the muons produced by the neutrinos interacting in the earth shield upstream. Even with a very conservative resolution time of 50 ns, the event overlap probability, as well as the random occupancy probability of any single strip, is considerably less than 10^{-3}.

4. The far detector

The MINOS far detector is a 5.4 metric kt magnetized iron calorimeter with scintillator as the active detector. The basic module is an 8 m diameter, 1-inch thick steel plane, followed by a scintillator plane. A MINOS supermodule is made up of 242 of these modules; two supermodules compose the baseline MINOS far detector. Each supermodule is energized independently by current in a 15 kA-turn coil so as to provide a toroidal magnetic field in the iron averaging about 1.5 T. An artist's sketch

of the far detector is shown in Figure 5.

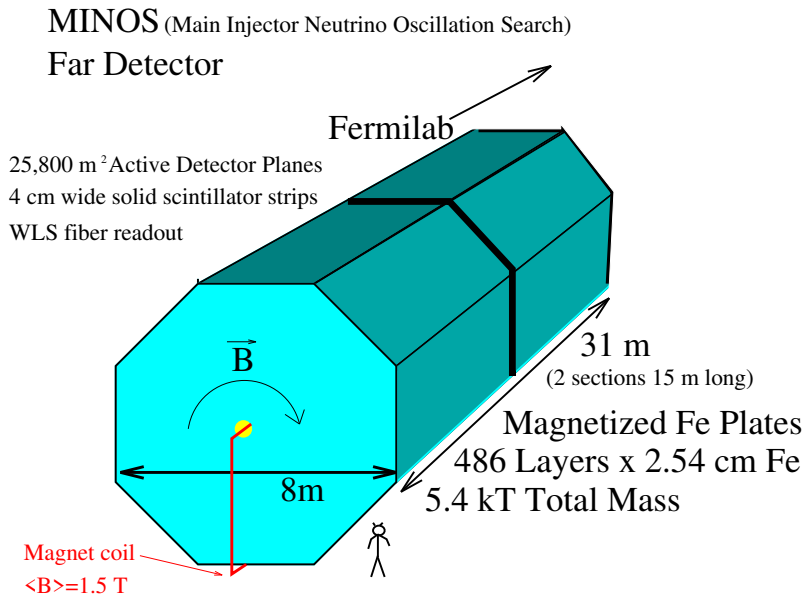

Figure 5: Sketch of the MINOS far detector.

Each scintillator plane is made up of 192 strips, each one 4 cm wide and up to 8 m long, depending on their location in the plane. The orientation of the strips alternates by $\pm 90^\circ$ in successive planes. Each scintillator strip has a wavelength shifting fiber imbedded in it to capture, wavelength shift, and transport the light to the two ends. Both ends of each fiber are coupled through clear fibers and multiplexing boxes to 16-channel multipixel photomultiplier tubes. Eight different fibers, from eight strips spaced roughly 1 m apart on the detector, are coupled to each pixel. The resultant 8-fold ambiguity can be resolved in software by utilizing the fact that the exact arrangement of which fiber is coupled to which pixel is somewhat different at the two strip ends. In addition, we will use timing and pulse height information from adjoining planes to provide independent ambiguity resolution.

We have constructed one plane and are in the process of building a four-plane prototype. The single plane, with magnetic field supplied by a set of wound cables, is shown in Fig. 6.

5. MINOS physics capabilities

In this Section we shall describe MINOS physics capabilities using Main Injector neutrinos. The potential measurements can be divided into three groups: statistical measurements, $\nu_\mu \to \nu_e$ identification, and study of exclusive τ decay channels.

The statistical measurements can be viewed as providing four independent quantities, namely the rates and energy spectra for both neutral current (NC) and charged

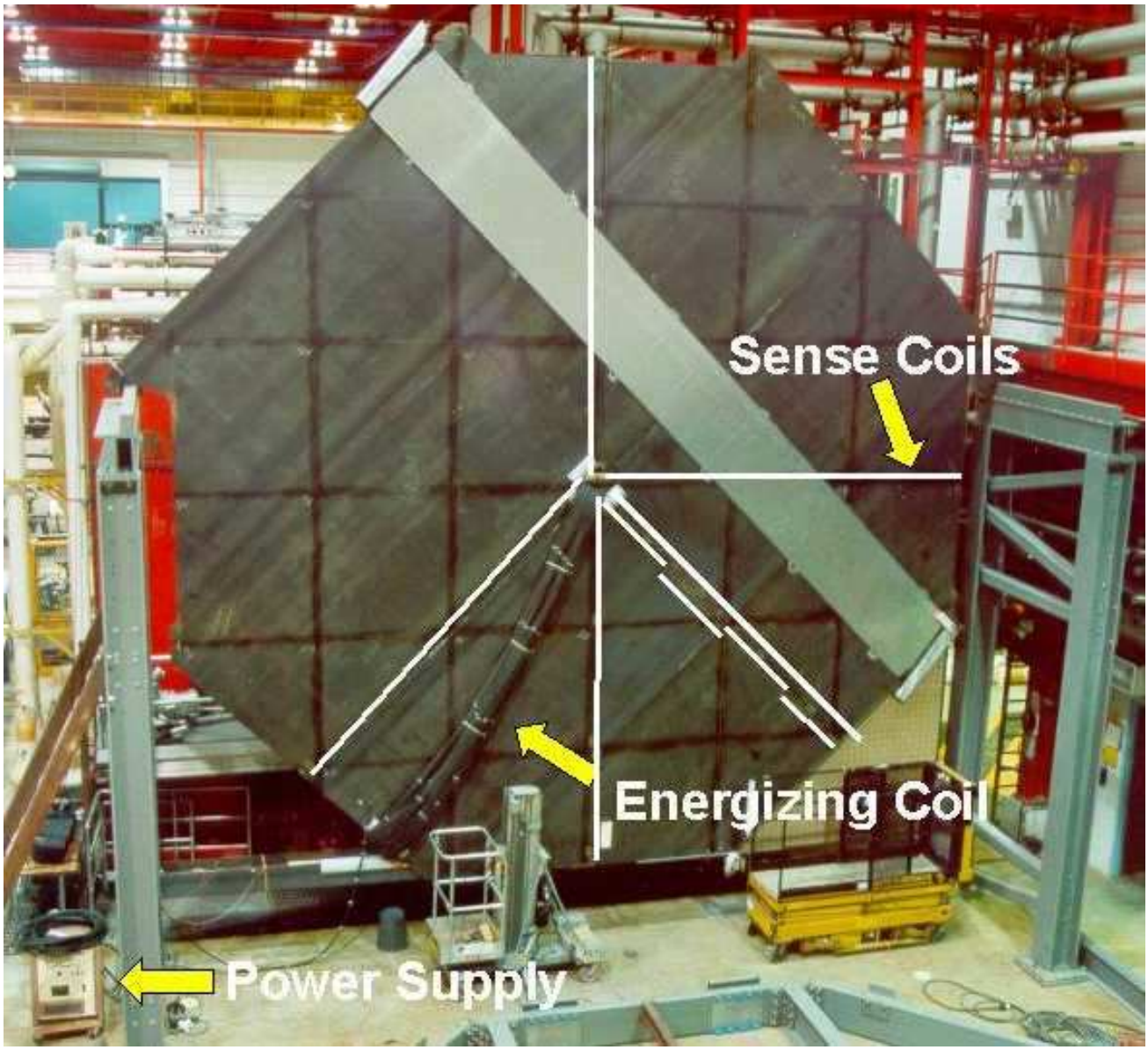

Figure 6: Photograph of a Single Far Detector Plane in the New Muon Lab at Fermilab. One counter module covers part of the plane. Cables used to generate the magnetic field are also shown.

current (CC) reactions. In practice, the event identification for this study is actually made by classifying events as either "short" or "long," but we use the NC/CC nomenclature as being roughly equivalent. Both rate and energy measurements of CC events yield results which are independent of the mode of oscillation. Any mode of ν_μ oscillations will result in the depletion of ν_μ CC events, and the CC energy spectrum can be used to measure the oscillation parameters. Comparison of CC energy spectra at the near and far detectors allows us to determine the relative fraction and the energy spectrum of the "missing" events. The size of the depletion is related to $\sin^2(2\theta)$ and their mean energy provides a measure of Δm^2. Figure 7 displays this effect for two different sets of the oscillation parameters.

As the third statistical measurement, we choose to use the ratio NC/CC, rather than the rate of the NC events themselves. This ratio has the advantage that it does not require understanding of the relative fluxes at the near and far detectors and thus is less subject to systematic errors. It is quite sensitive to oscillations because, not only are the CC events depleted, but the NC events are enhanced, since most of the ν_τ and all of the ν_e events created through oscillations will add to the NC category.

The power of the NC-event rate and energy spectrum measurement has been demonstrated by the CCFR experiment[10], which has been able to set a limit on $\sin^2(2\theta)$ of 2.7×10^{-3} (1.9×10^{-3}) for $\nu_\mu \to \nu_\tau$ ($\nu_\mu \to \nu_e$) oscillations in the region of Δm^2 corresponding to their maximum sensitivity. The NC measurements, when combined with the CC measurements, are able to identify the relative contributions of the different oscillation modes.

MINOS has excellent capability to distinguish ν_μ and ν_e CC events from NC events based on the shapes of hadronic and electromagnetic showers. The ν_e CC events will deposit most of their energy early in the shower, and the transverse width of the shower will be significantly narrower than for the hadronic shower of the NC events, which constitute the main background. The CCFR experiment[11] has already demonstrated that at high energies one can identify the ν_e CC events by the longitudinal shape alone, even with 10 cm thick iron plates. Our sensitivity to $\nu_\mu \to \nu_e$ oscillations using this method will be limited mainly by the statistical fluctuations in the number of ν_e CC events expected in the far detector due to the ν_e component in the beam (although this component is small, it is the limit for this mode).

The MINOS sensitivities obtained by different methods, at the 90% confidence level, for both $\nu_\mu \to \nu_\tau$ and $\nu_\mu \to \nu_e$ are shown in Figure 8. The limit curves shown correspond to a 10 kt-yr (before fiducial cuts) exposure of the far detector in the high-energy wide-band beam, using realistic fiducial volume cuts. The assumed 1% systematic error limits the sensitivity of the near-far rate comparison test.

Recently we have begun to study signal-finding using more sophisticated techniques. There are two problems with the usual methods:

1. Using χ^2-based statistics suffers from the problem endemic to the χ^2: it is indifferent to shape and will judge a distribution systematically low by 1σ to be

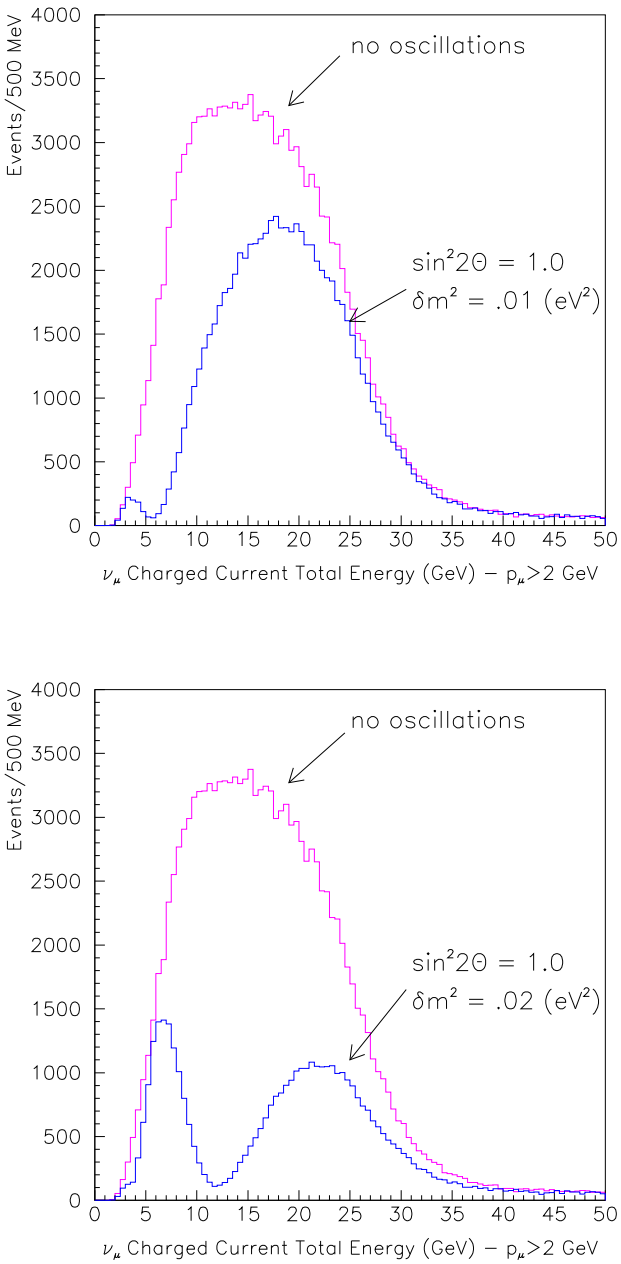

Figure 7: Energy spectrum of reconstructed ν_μ^{CC} events in the MINOS far detector in the case of no oscillations, compared to the spectra obtained for oscillations with $\Delta m^2 = 0.01$ eV^2 (top) and $\Delta m^2 = 0.02$ eV^2 (bottom). The high-energy WBB has been assumed, and the spectra have been smeared by expected detector resolution.

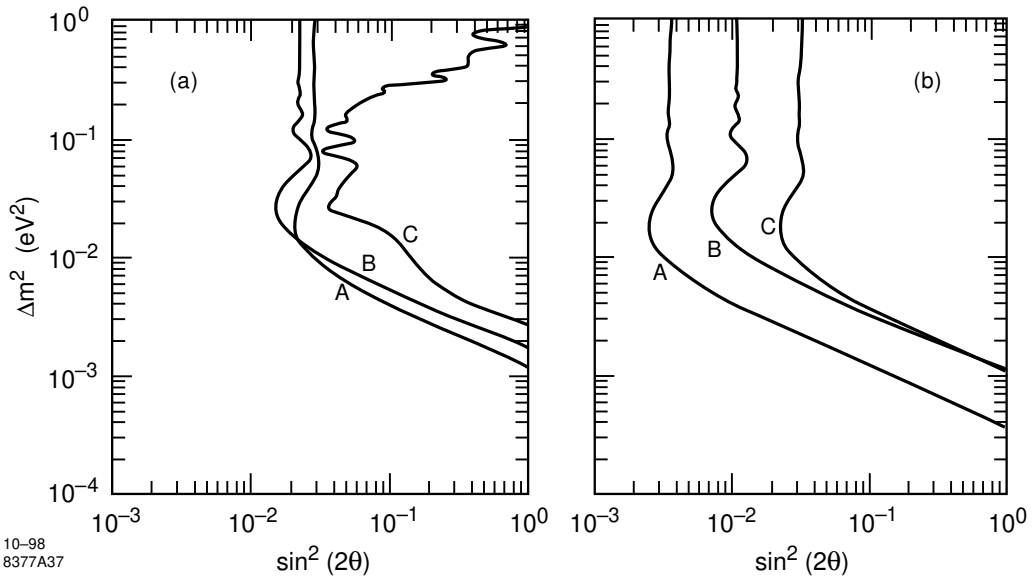

Figure 8: 90% confidence level limits on neutrino oscillation parameters which would be established by MINOS with 10 kt-years in the absence of oscillations, using the high energy wide band beam. The A, B and C curves show limits obtained from different oscillation tests. (a) $\nu_\mu \to \nu_\tau$ limits, where curve A is for the near-far event rate comparison, B is for the NC/CC ratio test, and C is for the CC-event energy test. (b) $\nu_\mu \to \nu_e$ limits, where curve A is for the electron appearance test, B is for the NC/CC ratio test, and C is for the near-far event rate comparison.

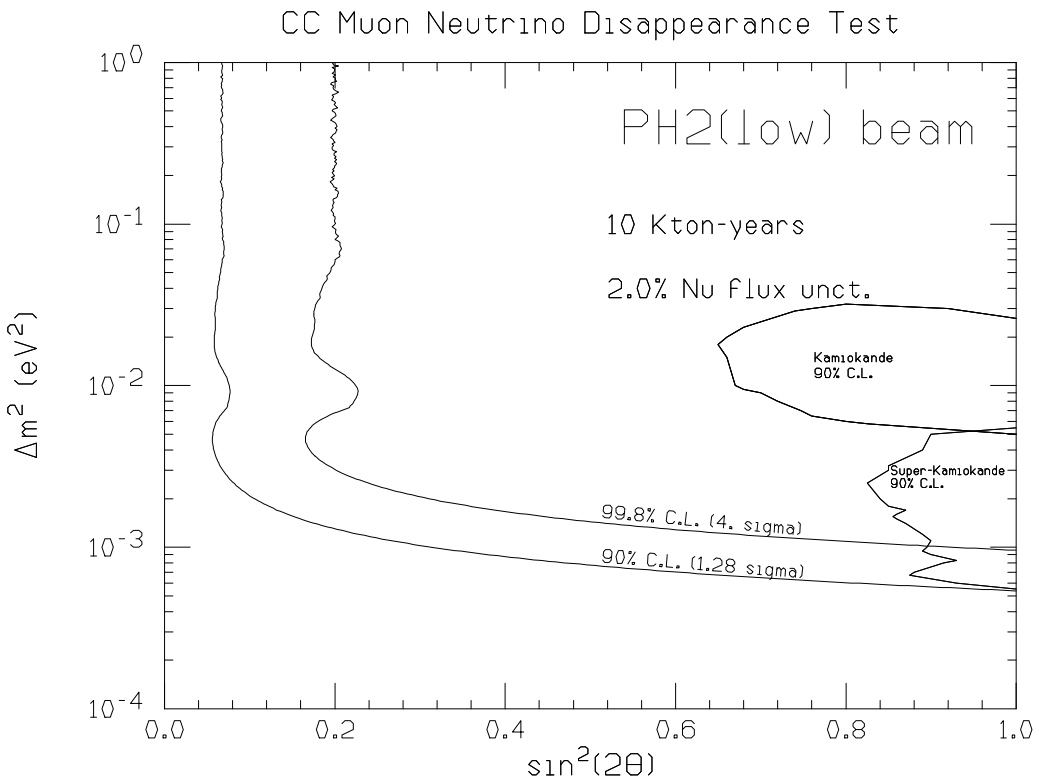

Figure 9: Sensitivity of the ν_μ disappearance test (90% CL limits and 4σ contour) for a 10 kt-yr exposure in the low energy PH2(low) neutrino beam.)

just as good as one randomly spread about the central value. The Kolmogorov-Smirnov statistic eliminates this problem.

2. Searches which find a "best-fit" and then vary by parabolic errors are incorrect near the physical boundary. The Feldman/Cousins prescription (known to mathematicians as Neyman-Pearson) eliminates this difficulty.[14,15)]

We present below preliminary estimates on the signal-finding capability of MINOS in two scenarios for the lowest-energy beam. Errors correspond to 10 kt×years. A reconstruction algorithm for charged-current muons has been applied.[16)] The flux has been allowed to vary by 2% overall (correlated) and by 2% in any 1 GeV bin (uncorrelated). The correct $y-$ distribution (calculated from GEANT) is included.

6. Schedule

Civil construction on the FNAL site is expected to start in early 2000. The Soudan Cavern excavation will begin in mid-1999 and end in early 2001. The first super-module will be operational in mid-2002, and data-taking can begin immediately. The full near detector will be finished at latest by late 2002 to early 2003 and data-taking will continue while the second super-module is installed, ending in mid-2003. The fiducial exposure for the experiment is 10 kt×years, or about two years later.

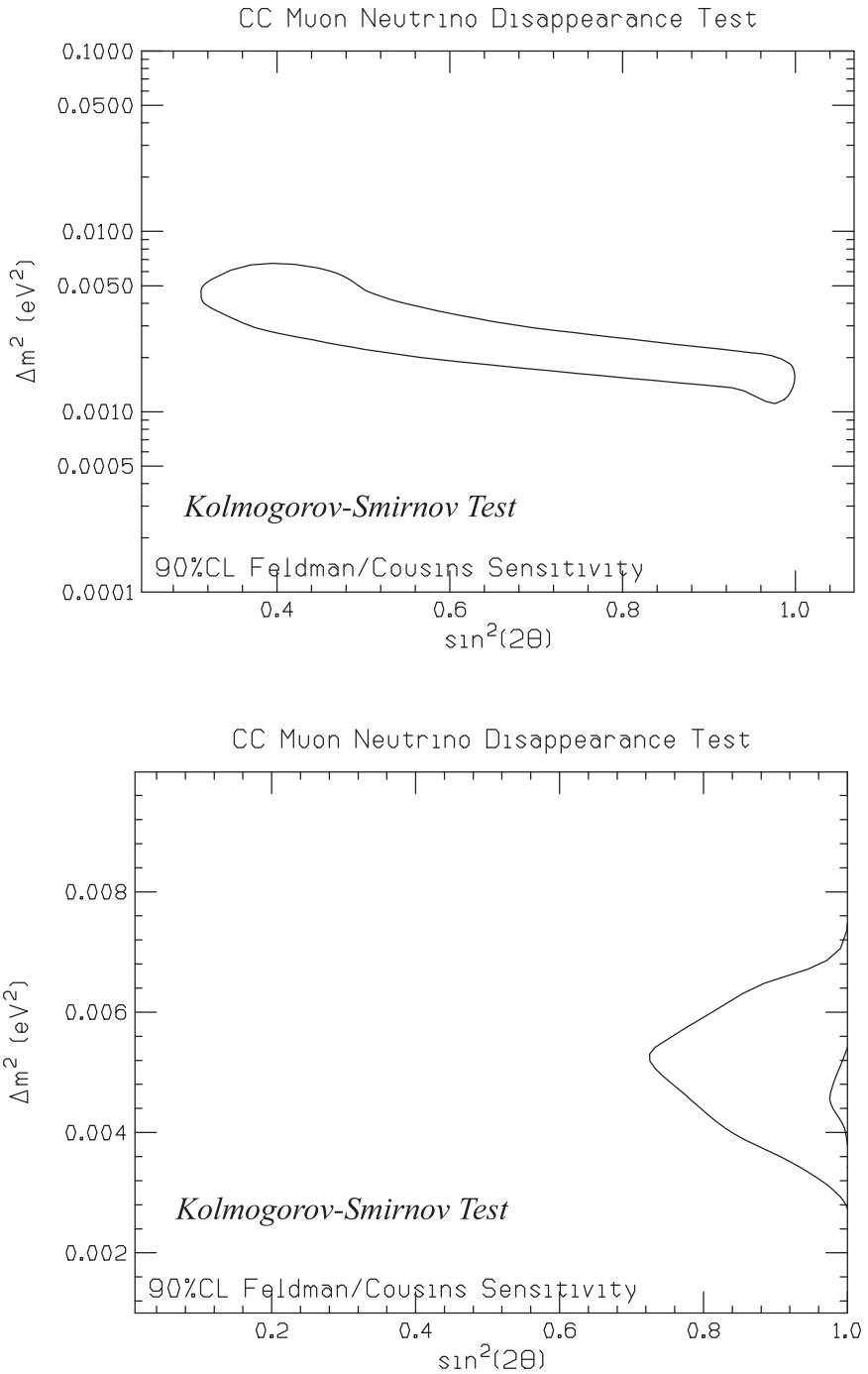

Figure 10: Sensitivity of the ν_μ disappearance test for Signals at $\Delta m^2 = 0.002, 0.005$ and $\sin^2 2\theta = 0.8$. (90% sensitivity for a 10 kt-yr exposure in the low energy PH2l neutrino beam. Note the scales vary in order to make the plots more informative.

7. References

1) The MINOS Collaboration, "The MINOS Detectors: Technical Design Report," October 1998, Fermilab Report NuMI-L-337.
2) The MINOS Collaboration, "P-875: A Long-baseline Neutrino Oscillation Experiment at Fermilab," February 1995, Fermilab report NuMI-L-63.
3) The MINOS Collaboration, "MINOS Physics Goals and Experimental Requirements," January 1997, Fermilab report NuMI-L-229.
4) "Report of the HEPAP Subpanel on Accelerator-Based Neutrino Oscillation Experiments," September 1995, DOE Office of Scientific and Technical Information Report No. DOE/ER-0662.
5) The MINOS Collaboration, "Neutrino Oscillation Physics at Fermilab: The NuMI-MINOS Project," May 11, 1998, Fermilab report NuMI-L-375.
6) The MINOS Collaboration, "MINOS Progress Report to the Fermilab PAC," October 1997, Fermilab report NuMI-L-300.
7) J. Hylen *et al.*, "Conceptual Design for the Technical Components of the Neutrino Beam for the Main Injector (NuMI)," September 1997, Fermilab-TM-2018.
8) The Fermilab NuMI Group, "NuMI Facility Technical Design Report," October 1998, Fermilab report NuMI-346.
9) The MINOS Collaboration, "MINOS Experiment R&D Plan: FY 1996-1998," June 1996, Fermilab report NuMI-L-184.
10) K.S. McFarland *et al.*, Phys. Rev. Lett. **75**, 3993 (1995).
11) A. Romosan *et al.*, Phys. Rev. Lett. **78**, 2912 (1997).
12) The MINOS Collaboration, "Status Report on τ Identification in MINOS," January 1997, Fermilab report NuMI-L-228.
13) The MINOS Collaboration, "Addendum to P-875: A Long-baseline Neutrino Oscillation Experiment at Fermilab," April 1995, Fermilab report NuMI-L-79.
14) G.J. Feldman and R.D. Cousins, Phys. Rev.**D57**, 3873 (1998).
15) An explanation accesible to particle physicists is given in G. Cowan, *Statistical Data Analysis* (Oxford: Oxford University Press, 1998, ISBN 0-19-850156-0).
16) D. Petyt, "A Study of Parameter Measurement in a Long-Baseline Neutrino Oscillation Experiment", Queen's College Ph.D. Thesis, RAL-TH-1998-008, June 1998.